Celestial Mechanics and Dynamical Astronomy manuscript No.
(will be inserted by the editor)

A study of low-energy transfer orbits to the Moon: towards an operational optimization technique

R. Capuzzo-Dolcetta · M. Giancotti

Received: date / Accepted: date

Abstract In the Earth-Moon system, low-energy orbits are transfer trajectories from the earth to a circumlunar orbit that require less propellant consumption when compared to the traditional methods. In this work we use a Monte Carlo approach to study a great number of such transfer orbits over a wide range of initial conditions. We make statistical and operational considerations on the resulting data, leading to the description of a reliable way of finding "optimal" mission orbits with the tools of multi-objective optimization.

Keywords Low-energy Orbits · N-Body · Restricted Problems · Spacecraft · Numerical Methods

PACS 95.10.Ce · 95.55.Pe

1 Introduction

When facing the problem of transferring a spacecraft from an orbit around the Earth to one around the Moon, the option usually taken is that of a two-impulse Hohmann transfer. The past two decades have seen the discovery and development of a new family of orbits that exploit the N-body dynamics to reduce the Δv budget of interplanetary missions. These "low-energy orbits" are rather new but have already been used several times to reach the Moon and the Earth-Sun libration points. Examples are the Japanese Hiten, the European SMART-1 and the NASA GRAIL missions.

The purpose of this work is to study how the different types of transfer orbits to the Moon compare to each other in terms of performance and room occupied in the space of the free parameters like the elements of the initial orbit and the launch

Roberto Capuzzo-Dolcetta
Dep. of Physics, Sapienza, Univ. of Rome,
E-mail: Roberto.Capuzzodolcetta@uniroma1.it

Marco Giancotti
Scuola di Ingegneria Aerospaziale, Sapienza Univ. of Rome,
E-mail: marco.giancotti@uniroma1.it

date. This is done with a Monte Carlo approach, producing a random population of transfer orbits within a wide range of initial conditions.

Section 2 briefly describes the dynamics of the 3- and 4-body problem which make the low-energy orbits possible. These are divided into the "outer" type and the "inner" type, rather different from each other. Section 3 describes the way the numerical simulation was performed, the initial conditions and the algorithm used. Section 4 contains an analysis of the Δv, the total duration and their dependence on the initial conditions of the transfer orbits. Section 5 describes how the data could be analysed with the methods of multi-objective optimization to search for the preferable type of transfer for a mission. Section 6 states the conclusions.

2 Types of Earth-Moon Transfers

2.1 The N-Body Problem

The study of the dynamics of a small body in the Solar System corresponds to searching the solution of a classical, Newtonian, $N+1$-body problem, where N is the number of gravitating bodies (Sun and planets) in the system, with given initial conditions.

The problem of flying a probe in the Solar System is that of a point of negligible mass that moves along the geodesic defined by its initial conditions in the time varying potential given by the revolving planets and the Sun. A precise integration of the equations of motion of the probe, even in the simplifying assumption of point mass particle, is obtainable by numerical methods once the right hand side (forces) is given through high precision ephemerides. The transfer of a spacecraft from the Earth to the Moon can be studied, at a high level of accuracy, as that of a body of negligible mass in the field of 3 finite mass bodies (Earth, Moon and Sun). Analytical solutions are only available in the case of triangular and rectilinear configurations. For generic applications, numerical methods are unavoidable.

The requirements characterizing the PCR3BP are:

- one of the three bodies is much smaller than the other two and its gravitational effect on them is negligible;
- the two larger bodies, which we will call the *primaries* A and B travel on circular orbits around each other;
- the third body, which we will call the *particle* P, moves in the plane of the primaries.

In particular, Joseph Louis Lagrange's work on the 3-body problem led him to the discovery of five points of equilibrium, sometimes called *libration points*, on which the whole system's dynamics is based.

The energy and momentum of the third body (P) are not conserved quantities when $N = 3$. The only first integral known in the PCR3BP is the *Jacobi integral* C, defined as

$$C = -2\Phi(x, y) - (\dot{x}^2 + \dot{y}^2)\,, \tag{1}$$

where $\dot{x}$ and $\dot{y}$ are the components of the velocity of P and $\Phi(x, y)$ is the effective potential, containing both gravitational and centrifugal terms. For any given value of C, the motion of the particle is spatially confined inside the so called *Hill region*,

$$\left\{(x, y) \in R^2 :\, C \leq -2\Phi(x, y)\right\}\,, \tag{2}$$

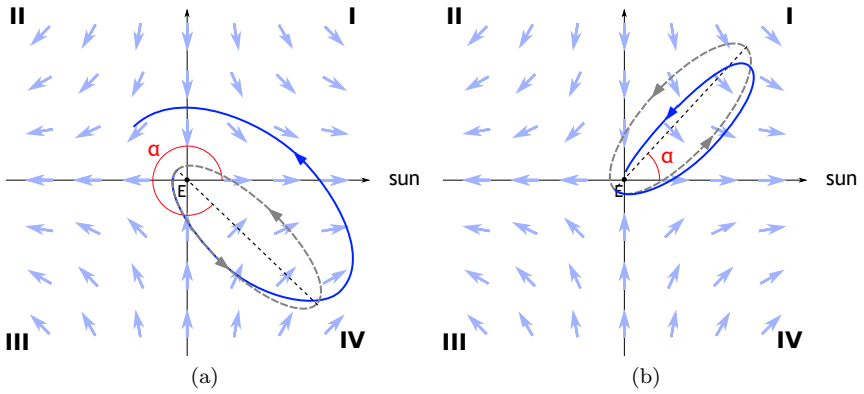

Fig. 1: The α angle and the shape of the gravity gradient induced by the Sun in the surroundings of the Earth. The direction of the Sun and the numbers of the quadrants (I, II, III, IV) are shown. (a) Deviation from the (initially osculating) Kepler orbit (dashed gray line) when α is in an even quadrant: the final perigee is higher than the initial one. (b) When α is in an odd quadrant, the length of the major axis is reduced, leading to a lower perigee.

bounded by *zero velocity curves* (ZVC), which have different shapes depending on the different values of C and of the system's masses.

2.2 Lunar Transfer and Low Energy Orbits

In the specific case of a transfer to the Moon, the two primary bodies in the 3-body formulation of the problem are the Earth and the Moon, while the spacecraft (P) is the third body. This system does not meet the requirements of the PCR3BP exactly. However it is close enough to display qualitatively equivalent solutions.

The traditional method of bringing a payload from the Earth to the Moon is through a Hohmann transfer which has a typical total duration T_t of 5 days (from LEO). This procedure requires a value of C lower than that of the 4^{th} and 5^{th} libration points, thus selecting a configuration of the Hill region where motion is allowed in the whole space, without forbidden regions. In this case the duration of the flight and the energy of the system allow us to ignore the complex dynamics tied to the libration points. Apart from later corrections for the various perturbations, this approach only makes use of 2-body celestial mechanics principles.

Recent research has led to the discovery of another family of trajectories exploiting the properties of the Hill region and of the libration points (Belbruno, 1987; Belbruno and Miller, 1990; Kawaguchi et al, 1995; Koon et al, 2000, 2001). In order to make this possible, C needs to be close to the critical values, confining the space of possible motion and thus allowing the spacecraft to be "captured" in the area around the Moon. Some of these trajectories can be achieved only if the Jacobi "constant" C varies throughout the flight. The intervention of a fourth body is therefore needed to provide an external perturbation to the 3-body system. These are sometimes called "low-energy orbits".

Influence of the Sun. The gradient of the solar gravitational field in the surroundings of the Earth is expressed, neglecting the second order terms, with the tidal tensor

$$\mathbf{\Phi} = \frac{GM_{sun}}{R^3}\left[3\hat{R}\hat{R} - \mathbf{u}\right]\mathbf{r}, \tag{3}$$

where $\mathbf{R}$ is the Sun-Earth distance vector, $\mathbf{u}$ the unit dyadic and $\mathbf{r}$ is the Earth-spacecraft distance vector. The field introduces a force pushing P away from the Earth along the Sun-Earth line and towards it in the direction orthogonal to it, as shown in Figure 1. The key parameter relating this effect to the dynamics of an elliptical orbit is the angle, α, between the Sun-Earth line and the orbit's major axis (Circi and Teofilatto, 2001). When α is inside the 2^{nd} or 4^{th} quadrants in the figure, the Sun's gravity field aids the orbit by rising the spacecraft's energy, especially when it is close to apogee (Figure 1a.). The opposite happens when α is in one of the other two quadrants, where the spacecraft's energy is lowered (Figure 1b.). The overall effect is an increase or decrease of the orbit's major axis growing non-linearly with its length.

It was found (Belbruno and Miller, 1990) that it is possible to exploit this phenomenon in order to design spacecraft trajectories that reach the Moon with lower relative kinetic energy, thus decreasing the overall fuel requirements of the mission. The spacecraft is "captured" gravitationally by the lunar field in a process called a *ballistic capture*.

Ballistic capture. Traditional Hohmann-type transfers approach the Moon with a relatively high velocity requiring the use of on-board rockets to slow down the motion of P until it becomes bounded to the Moon. In order to obtain a stable, bound orbit around the Moon, the energy of the spacecraft with respect to it must be decreased to negative values. In the case of the 3-body problem, the condition is $C > C_1$, where C is the Jacobi constant of the spacecraft and C_1 is that related to the first libration point L_1. This corresponds to closing the L_1 neck of the Hill region so that passage between the Earth and Moon domains of possible motion is blocked and P is confined in the region around the Moon.

With ballistic capture, the spacecraft approaches the Moon with a low relative velocity and enters directly into a temporarily bound orbit. An example of ballistic capture in nature is that of some comets in the combined Sun-Jupiter gravitational field. Most famous is comet 39P/Oterma, which was captured for a short time around Jupiter in 1936.

It must be noted that the chaotic 3-body dynamics of the system allows, generally, for a temporary (unstable) ballistic capture, although it is thought that permanent capture (i.e. the probe remains bound to the Moon forever) can happen (Belbruno, 2004). Normally, after the ballistic capture transfer, the spacecraft performs one or more revolutions around the Moon before escaping again into one of the other realms of possible motion. For this reason an active maneuver is necessary to stabilize into a lunar orbit. The clear advantage of using this type of trajectory lies in its lower fuel requirements with respect to usual Hohmann transfers.

Outer transfer. The contribution of the Sun described above can be used to naturally modify the shape of a highly eccentric orbit. This is the case already shown in Figure 1. When the apogee distance r_a is close to 1.5×10^6km, the effect becomes

strong enough to raise the successive perigee up to about 4×10^5 km. When this happens, the spacecraft can approach the Moon with a lower relative velocity than a Hohmann transfer, possibly resulting in a ballistic capture. In this paper this type of trajectory is called *outer transfer*.

The advantage of this type of transfers, when ballistic capture occurs, is the reduced Δv in the final phase, when propulsion is needed to stabilize the orbit. The data analyzed in the following paragraphs shows that this method results in a reduction of up to 44% of this second impulse compared to that of a Hohmann transfer.

Inner resonance transfer. A second type of low-energy transfers does not make use of the effect of the Sun. Instead, it is based on the unstable dynamics near the Earth-Moon L_1 libration point. In this case, which we will call *inner resonance transfer* or inner transfer, the apogee distance r_a produced by the initial Δv lies inside the orbit of the Moon, roughly 3.30×10^5 km from the Earth. The duration of the transfer T_t goes from 85 days upwards, depending on how many Earth orbits are completed before falling into the Moon's area of influence.

In these transfers the effect of the Sun is much weaker and it doesn't help in *raising the apogee* up to the lunar distance, even during the "favorable" α quadrant epochs. Yet its contribution can be important when α is in one of the other two quadrants, because it can *lower the perigee* enough to make the spacecraft impact the Earth.

The process by which the capture occurs despite the "short apogee" is the execution of one or more *resonance hops* with respect to the Moon. Each time the spacecraft flies by L_1 its trajectory can shift into a new near-resonant state, usually with a longer major axis. This is repeated until the spacecraft is able to enter the Moon's sphere of influence. The dynamics behind these resonance hops is tied to the structure of phase space when P is close in energy and position to L_1 (Belbruno and Marsden, 1997; Belbruno, 2008). However its details are still not completely understood.

Interpretation The explanation given above involving tidal forces and the α angle (Circi and Teofilatto, 2001) is only one of several. The original rigorous interpretation of the phenomenon is given in Belbruno (1987), Belbruno and Miller (1993), Bello Mora et al (2000) through the concept of weak stability boundary. This is the region where the gravitational forces due to the various bodies are similar, allowing for ballistic capture and propellant savings.

Another insightful interpretation involves the stable and unstable manifolds related to the periodic orbits at the collinear libration points (Conley, 1968; Koon et al, 2000, 2001). The phase space position of the spacecraft with respect to these two manifolds determines its qualitative behavior in the framework of the 3-body problem. By choosing carefully the initial conditions of the orbit it is possible to build complex paths going around several celestial objects with few or no active maneuvers.

3 Method

The approach followed in this work is statistical, through the search of generic transfer orbits from a low Earth parking orbit to a stable lunar orbit. The nature of the simulation makes it possible to study the complete phenomenology of the transfer problem, eliminating any technical or theoretical bias that could be included in an ad-hoc algorithm. The aim is to contribute a slightly more complete picture of the phenomenology of the transfers, rather than discovering new methods to create low-energy orbits.

The simulations are performed using a restricted version of the Solar System consisting of Earth, Moon and Sun. They are modeled, in the basic settings, as point masses with realistic, non-planar motion, taken from the ephemerides of the Jet Propulsion Laboratory's Horizons System[1]. The other planets are not considered in the present research because they introduce negligible effects in the short term.

3.1 Initial Conditions for the Orbits

Each transfer is made of two separate ignitions: Δv_1 to begin the transfer at time t_0 and Δv_2, at time t_2, to inject the spacecraft into a stable orbit around the Moon. The initial condition *for all the transfers* is a circular low Earth parking orbit with a radius $r_0 = 6720$ km, and Δv_1 is always applied in a direction parallel to the instantaneous velocity [2].

The ecliptic coordinate system (x_{ec}, y_{ec}, z_{ec}) is assumed for the rest of this paper, unless differently stated. The inclination of the plane of the (circular) parking orbit can be varied using two angular parameters: θ, the angle of rotation around the x_{ec} axis and ν, the angle of rotation around the y_{ec} axis. The angle of rotation around the z_{ec} axis is never changed.

Being the parking orbit circular, the argument of perigee is not defined, and the initial conditions for the satellite motion leaving the parking orbit are given on the crossing of the parking orbit plane and the ecliptic. This is the only strong restriction given to the initial conditions. It greatly reduces the parameter space that is explored, but also makes the number of necessary calculations manageable.

Δv_1 is chosen randomly in an interval between a specified minimum value (different choices were tested) and a maximum value that corresponds to the escape from the Earth's gravitational well starting from the parking orbit, i.e. $\Delta v_1 = 3.19$ km s^{-1}. After the boost, the trajectory is integrated forward in time for a period of 160 days. Among the orbits thus produced, all those that do not enter the sphere of radius 10^4 km around the Moon are discarded. Only those passing closer to the Moon than 10^4 km without colliding with it are stored.

After this first screening the algorithm applies a 2-impulse Hohmann maneuver to reach a stable 2000 km circular orbit around the Moon (an altitude of 262 km). The first impulse of this maneuver is performed at the point closest to the Moon of the 160-day orbit. The portion of the trajectory that comes *after* this point of closest approach is discarded. The result is an elliptic orbit with periselenium

[1] http://ssd.jpl.nasa.gov/?horizons

[2] Note that a high trust propulsion capable of instantaneous bursts is assumed.

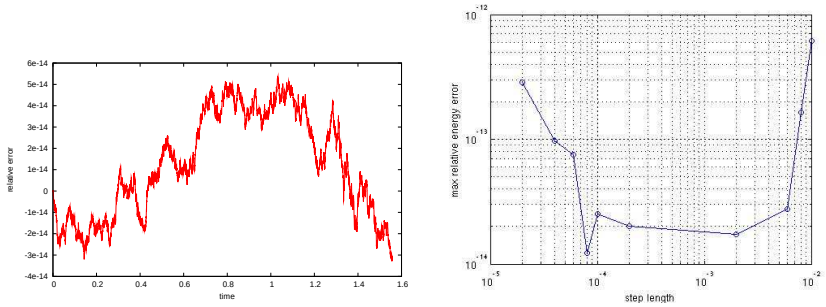

(a) (b)

Fig. 2: (a): relative error in energy in the orbital integration for an orbit lasting 93 days (time is in system's units). (b): maximum relative error in energy over a full orbit, relative to different lengths of the time step.

distance of 2×10^3 km. The other impulse is done at periselenium and it circularizes the orbit. In total these two maneuvers require a variation of velocity indicated as Δv_2.

3.2 Orbital Integration

The integration of the equations of motion of a spacecraft submitted to a variable external potential with given initial conditions must be of the highest possible precision. Anyway, it is well known that ordinary numerical methods for integrating Newtonian equations of motions become dissipative and exhibit incorrect long term behavior (see, e.g., Menyuk (1984); MacKay (1992); Cartwright and Piro (1992)). This is a serious problem performing N-body computations, particularly when studying the evolution of systems over large time intervals.

One possible solution is using symplectic integrators, which are a particular type of *geometric* integrators which, respect to ordinary integrators, have the advantage to be qualitatively better because they preserve the physical properties of the original, although discretized, system's hamiltonian. This allows for a good conservation of the characteristics of the dynamical system's time flow properties, thing that is particularly appreciated when the simulation is performed over an extended time, with an energy error much better constrained than with ordinary methods which show an irreversible drift. The advantage of using a symplectic algorithm of sufficiently high order is that it gives more reliability of the quality of the results at a computer time consumption similar to that of a non-symplectic method, so to make it worth using also for integrations limited in time.

The choice of symplectic methods is wide, for it is possible to construct high order integrators (Yoshida, 1990). For the purposes of this paper, we used the 6^{th}-order explicit scheme whose coefficients are taken from the first column of the Table 1 (SI6A) of Kinoshita et al (1991), which leads to a conservation of energy by a factor 50 better than with the other two possible sets of coefficients reported in the same Table. The integration of the spacecraft orbits in the external field was done by mean of a properly adapted version of the full N-body code NBSymple,

developed by Capuzzo-Dolcetta et al (2010). The code was also adapted to include a multipolar expansion (up to the 4th degree) for the Sun and the Earth potential and to account for the influence of the whole set of planets in the solar system, but these features were not used for the final computations.

Although the potential of the Sun is conveniently represented by a truncated multipolar expansion, accounting for its deviation from spherical symmetry, it is easily seen that the contribution of the quadrupole and hexadecapole (P_2 and P_4 Legendre's terms, respectively) contribute for a fraction of only about 7×10^{-12} to the solar gravitational force at one Astronomical Unit. Also the lunar potential, at the distances from the Moon of interest for this paper, is sufficiently well represented by the monopole term, as can be seen by comparing it to higher moments as deduced from the Lunar Prospector mission by Han et al (2011). So in the following calculation we considered, as absolutely sufficient for the scopes of this paper, just the solar, Earth and Moon monopole term in their gravitational potential.

The orbit of the point-like spacecraft is integrated with a maximum relative error of 2×10^{-14} (see Figure 2). When the time step is within the range $10^{-4} \leq \Delta t \leq 3 \times 10^{-3}$, our code, working on a standard Intel Xeon CPU is able to generate in one minute ~ 250 orbits with a duration of 160 days.

Further details on the numerical N-body code structure and characteristics can be found in Capuzzo-Dolcetta et al (2010).

4 Results

The method employed in the simulation explores a wide portion of the parameter space of the Earth-Moon transfer problem. Several kinds of orbits linking the two astronomical bodies are found. As it might be expected, most of the trajectories found are of limited applicability, with very large Δv and long durations. However, a significant number of "effective" trajectories, i.e. viable to practical utilization, exists. Besides the traditional Hohmann-like transfers, they also include the two types of low-energy transfers that exploit the 3- and 4-body dynamics of the Earth-Moon-Sun system (inner and outer types, described above).

A total of 5733 complete transfer trajectories were produced with the following 4 main simulation modes:

A. Progression of dates: several transfers each day during the course of one year. Lower limit on Δv_1 is such that the minimum r_a of the transfer orbit is $r_{a,min} = 3.3 \times 10^5$ km. This includes the Hohmann transfers and the inner and outer low-energy transfers. Angles ν and θ are both 0.
B. Progression of dates: like point 1, but the lower limit on Δv_1 is such that $r_{a,min} = 8 \times 10^5$ km. This *excludes* the Hohmann and inner transfers.
C. progression of values for ν; lower limit on Δv_1 such that $r_{a,min} = 8 \times 10^5$ km.
D. progression of values for θ; lower limit on Δv_1 such that $r_{a,min} = 8 \times 10^5$ km.

The choice of parameters is aimed both at exploring a wide spectrum of possibilities and at increasing the number of low-energy orbits to study. Most of the orbits were produced with the first two modes.

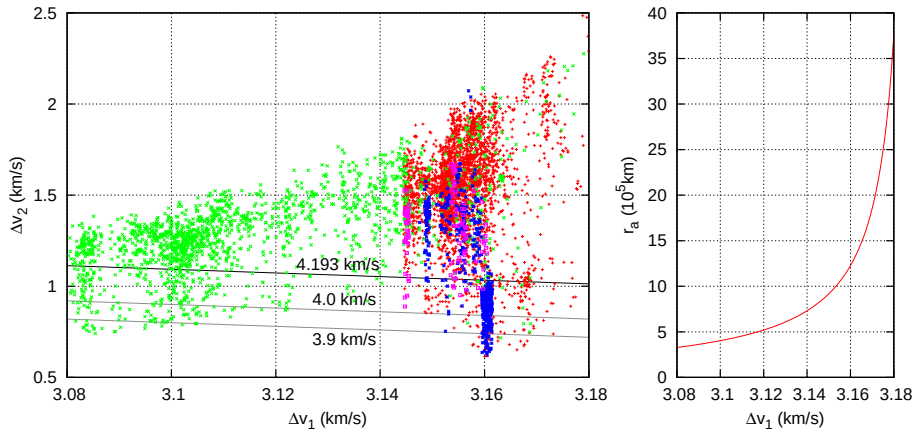

Fig. 3: Left: distribution on the Δv_1-Δv_2 plane of 5733 transfers. Green markers: simulation mode A (see text); red: mode B; magenta: mode C; blue: mode D. Lines corresponding to the equation $\Delta v_{tot} = \Delta v_1 + \Delta v_2 = k$ for three different values of k (as labeled) are shown. Right: relation between r_a of an elliptical Kepler orbit and Δv_1, given the initial conditions employed in the simulation.

4.1 Discussion on the Relation Between Δv_1 and Δv_2

A first aspect of the data produced by the simulations is the dependence of the second impulse (Δv_2) on the first (Δv_1). Δv_1 is only allowed to vary between 3.08 km s^{-1} and 3.19 km s^{-1} (the value necessary to reach the escape velocity), which results in apogee distances ranging from $r_{a,min} = 3.3 \times 10^5$ km to infinity (the extreme case being a parabolic orbit). Δv_2, on the other hand, ranges roughly from 0.7 to 2.0 km s^{-1}.

The left panel of Figure 3 shows a collection of orbits produced for different simulation modes. On this plot, an average Hohmann trajectory is located in the proximity of the point [3.100 km s^{-1}, 1.093 km s^{-1}]. Different markers denote the orbits produced with different modes (see figure caption). Note that the magenta and blue points are not as spread out as the other two modes because they were all simulated starting from the same initial date, during a favorable quadrant of α.

The curve in the right panel of Figure 3 shows, for reference, the relation between r_a and Δv_1 given the initial conditions in use. Note that the Earth-Moon distance is $\sim 3.85 \times 10^5$ km and the apogee of an outer orbit is $r_a = 1.2 \sim 1.5 \times 10^6$ km.

Main strip. The distribution in Figure 3 displays a direct positive correlation between Δv_1 and Δv_2 up to $\Delta v_1 = 3.140$ km s^{-1}, which corresponds to $r_a = 7.4 \times 10^5$ km. In this region the distribution takes the shape of a strip with increasing values of Δv_2.

For larger values of Δv_1, the distribution becomes widely scattered, branching also towards lower values of Δv_2. Most of the transfers on the main strip, excluding those in the lower-right area, are inefficient versions of Hohmann transfers and

many of them perform several revolutions before coming close to the Moon. The reason for this "Hohmann strip" in Figure 3 is straightforward, best explained by separating the cases in which Δv_1 is greater than or less than that of the theoretical Hohmann which we will here call Δv_1^h:

A. $\Delta v_1 > \Delta v_1^h$: here the transfer orbits cross the lunar orbit and go beyond it for a while instead of being tangent to it. Trajectories resulting from higher Δv_1's will therefore approach the Moon with wider angles with respect to the lunar instantaneous velocity. The higher this approach angle is, the higher Δv_2 needs to be in order to attain a stable final orbit;
B. $\Delta v_1 < \Delta v_1^h$: a traditional Hohmann transfer is not possible because the elliptic orbit does not intersect or touch the Moon's trajectory. However the passage of P close to the first libration point activates complex 3-body dynamics that can lead to a lunar orbit. In particular, most of these orbits perform resonance hops, increasing the length of their major axis and eventually falling into a ballistic capture around the Moon. The resulting Δv_2 used to stabilize the orbit is usually lower than that of a Hohmann transfer, and in some cases similar to that of an outer transfer.

Distribution for higher Δv_1. For $\Delta v_1 > 3.140$ km s^{-1}, the line of the distribution in Figure 3 expands also to low values of Δv_2. The upper portion is a continuation of the previously described Hohmann strip, while the lower branch is composed of low-energy outer transfers.

The difference between the two branches can be entirely ascribed to the 4-body dynamics due to the Sun, which becomes important when the point of apogee reaches the implied large distances from the Earth. The upper branch is dominant when the α angle between the Sun, the Earth and the orbit's apogee is unfavorable, i.e. in the 1^{st} or 3^{rd} quadrants. Conversely, when α is in the 2^{nd} or 4^{th} quadrants, the probability of obtaining an outer low-energy transfer is higher, producing the lower branch.

All the points of the lower branch around and below the $\Delta v_{tot} = 4.0$ km s^{-1} diagonal line represent outer low-energy transfers. The lowest value reached is $\Delta v_2 \simeq 0.61$ km s^{-1}, that is, 44% less than the Δv_2 of the *average* Hohmann transfer.

4.2 Transfer Duration and Δv

Two of the most relevant parameters to be taken into account in the choice of the transfer orbit for a mission are the total propellant consumption, expressed through Δv_{tot}, and the total time of flight, T_t. Depending on the specific purpose of the mission, greater importance may be given to one parameter over the other. The propellant used grows exponentially with the Δv of a maneuver, and from the point of view of the budget it should be kept as low as possible. On the other hand, missions that take a long time to reach the target can be unacceptable for various reasons, like life support costs in manned missions and related risks.

The plot in Figure 4 shows the distribution of the orbits in the Δv_{tot}-T_t plane. The orbits are produced with different choices of the t_0, ν angle and of the lower limit to r_a (displayed in the plot with different markers). Figure 4 can be used

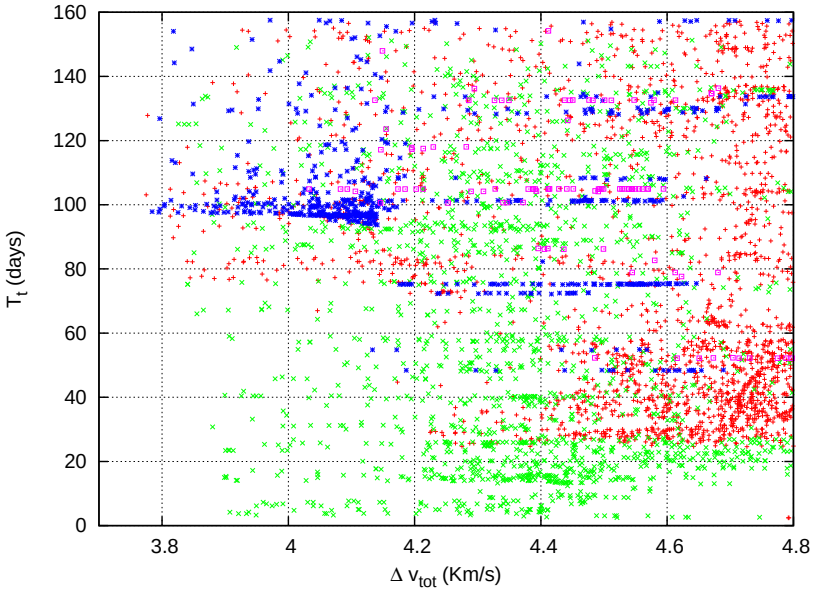

Fig. 4: 5733 transfers in the Δv_{tot}-T_t plane. The same symbols as Figure 3 apply.

as an aid in the choice of an optimal trajectory given a specific mission, a topic explored in more detail in Section 5.

4.3 Dependence on the Launch Date

The data obtained from the simulation show that the date of launch influences the Δv of the transfer orbits. The Moon needs to be in an appropriate part of its orbit in order to be reached by the spacecraft, and the required position is different for the various types of transfers. The dependence on the lunar cycle is evident in the obtained data from the oscillation of the probability of transfer with a period of 27.3 days, i.e. the period of the Moon's revolution around the Earth.

The second major effect is given by the angle α between the apogee and the Sun (described in Sect. 2). The gradient of the Sun's gravitational field around the Earth's position results in a tidal force acting on the orbiting body, whose direction depends on the angular configuration of the Sun-Earth-spacecraft system.

For short-term orbits, like the traditional Hohmann transfers taking 3 to 5 days to reach the Moon, the consequences of this force are negligible. However the contribution of the Sun cannot be overlooked when considering trajectories with r_a greater than that of the Moon, with $T_t \geq 80$ days. By changing the shape of the orbits, the Sun affects the velocity with which the spacecraft passes close to the Moon. The result is a variation in the Δv_2 needed to enter a stable lunar orbit.

This is visible in Figure 5, where Δv_{tot} for different launch dates is shown along with the periods in which α is in its various quadrants. Note that the date shown for the points is when Δv_1 is applied; a spacecraft in a low-energy orbit

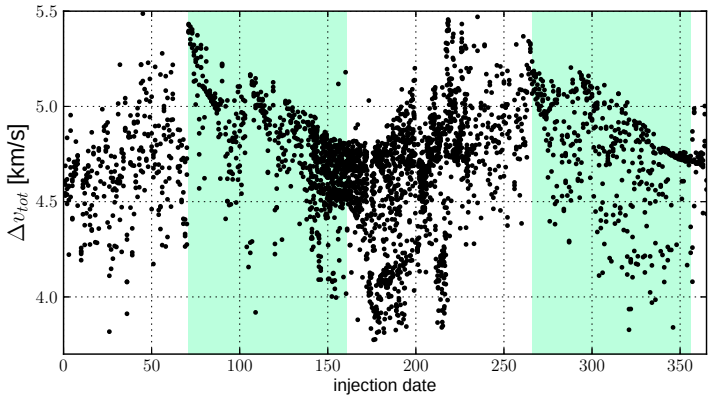

Fig. 5: Dependence on the launch date for a set of orbits with $\Delta v_1 > 3.14$ km s^{-1}. The "unfavorable" quadrants (1$^{\rm st}$ and 3$^{\rm rd}$) are shown on a darker background.

comes close to apogee, feeling the effect of the Sun, after roughly 30 to 70 days. Therefore, despite the appearance, the crests and troughs of the distribution do correspond to the predicted α phases (Circi and Teofilatto, 2001). Also, the most efficient orbits of the distribution are all located in the favorable quadrants of α, as will be shown in Section 5, Figure 10.

Of all the transfers with $\Delta v_2 < 1.0$ km s^{-1}, 93% have the apogee angle α inside either the 2^{nd} or the 4^{th} quadrant. The transfers happening when α is at the boundary between two quadrants ($\alpha = k\,\pi/2$ with $k = 1, 2, 3, 4$) display deformed shapes, because of the different effects of the Sun's gradient along the orbit.

Inner resonance transfers, with $r_a < 4{\times}10^5$ km do not show a clear dependence on α. The mechanism leading to a ballistic capture is, in this case, different and mostly independent of the position of the Sun.

4.4 Low-Energy Orbits

Existence of low-energy orbits. Taking into account different initial conditions (i.e. the A, B, C and D modes described earlier) the number of orbits found to be low-energy transfers constitutes a non negligible fraction of the total. The probability of producing a low-energy transfer when shooting in a given interval of Δv_1 is represented in the histogram in Figure 6. There is no rigorous definition of low-energy transfer, but putting an upper limit on the Δv_{tot} allows us to exclude the Hohmann and the other high-cost transfers. Considering that the average Hohmann transfer in this study has $\Delta v_{tot} = 4.193$ km s^{-1}, we can improvise two alternative definitions, one requiring $\Delta v_{tot} < 4.0$ km s^{-1} and another, stricter one requiring $\Delta v_{tot} < 3.9$ km s^{-1}.

Figure 6 shows the portion of all the orbits, in each bin of Δv_1, that fall into these two definitions. In both cases the low energy orbits exist in two separate

groups, as expected from Section 2: one for low values (inner transfers) and one for high values (outer transfers) of Δv_1. For both definitions there exists a gap between the two groups where no conforming transfer takes place.

The distribution of the transfers in Δv_1 can be translated into ranges of apogee distances. The inner transfers thus have apogee distances approximately 3.36×10^5 km $< r_a < 3.43 \times 10^5$ km. Outer transfers, on the other hand, exist in the range 1.23×10^6 km $< r_a < 1.31 \times 10^6$ km. Most of the optimized orbits described in other works go further out, up to 1.5×10^6 km from the Earth. The fact that these longer orbits are rare in this (non-optimized) simulation is certainly due to the greater difficulty in producing them. They occupy a smaller volume in the space of the parameters and therefore our Monte Carlo approach is less likely to find them. Of course, this more sensitive dependence on the initial conditions is the trade-off necessary to obtain higher efficiencies.

The plots of Figure 7 illustrate the Δv distribution of two sets of orbits of interest. The "inner set" is composed of all the transfers with $\Delta v_1 < 3.10$ km s^{-1} (the value of the mean Hohmann transfer), while the orbits of the "outer set" have $\Delta v_1 > 3.140$ km s^{-1}. Note that these two sets contain both low-energy and high-energy orbits.

For both sets the majority of the orbits have high Δv_{tot}, greater than 4.0 km s^{-1}, indicating high-energy orbits. However the left tails of both distributions extend down to 3.8 km s^{-1}, where the low-energy orbits are.

Examples of low-energy orbits. Five different low-energy transfers found in the simulation are shown in Figure 8. Orbits 8(a) to (d) are outer transfers. 8(a) has $i = 0$ from the start, while the following three (shown projected on a plane normal to the ecliptic) have different initial inclinations. Note that when displayed from above the ecliptic, these four transfers all have essentially the same shape. Their

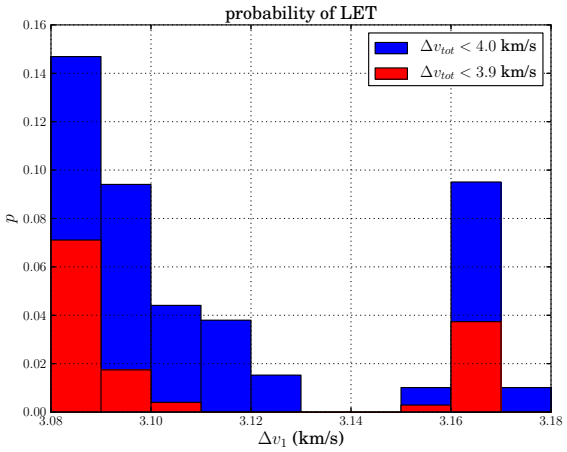

Fig. 6: Histogram showing the portion of orbits that are low-energy, using two alternative definitions based on Δv_{tot}.

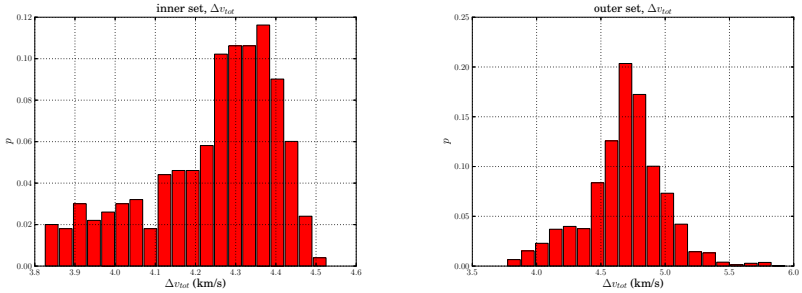

(a) (b)

Fig. 7: Δv_{tot} of the inner and outer sets of transfers. The count is normalized so that the sum is unitary. (a) inner set, 499 orbits, $\Delta v_1 < 3.10$ km s^{-1}; (b) outer set, 3538 orbits, $\Delta v_1 > 3.14$ km s^{-1}

independence to the initial inclination is due to the nature of the sun's tidal force, described in Section 2, constantly pulling towards the ecliptic plane.

Figures 8(e) and 8(f) show the same inner transfer in the inertial and in the Earth-Moon rotating frame. The sudden changes in the semi-major axis and eccentricity, due to resonance hops, are clearly visible.

5 Application of Multi-Objective Optimization Methods

Like most modern day design problems, the choice of an optimal trajectory for a space mission has to take into account a number of contrasting objectives, and thus belongs to the category called *multi-objective optimization* (MOO).

MOO studies the functional relation between the *search space*, that is the space of all the problem parameters, and the *objective space*, composed by the functions that quantify all the objectives. Every objective is translated into one "objective function" (Miettinen, 2001).

If there is only one objective, the best solution is the one maximizing or minimizing a suitable objective function, depending on the nature of the problem. When the number of objectives is greater than one, however, the conflict between them makes some kind of trade-off necessary. The concept of *domination* of one solution over another is introduced to identify which is preferable (or at most equal) in terms of all the objectives at the same time. The set of all solutions that are not dominated by any other solution, and therefore best under at least one objective, is called Pareto frontier or Pareto-optimal set (Miettinen, 2001).

5.1 MOO for Earth-Moon transfers

Normally, multi-objective optimization programming starts from the search space and uses an algorithm to find the optimal points in the objective space. Such operation is *not* performed in this work because a different approach has been chosen for the reasons detailed in the preceding sections. Nevertheless, the production of

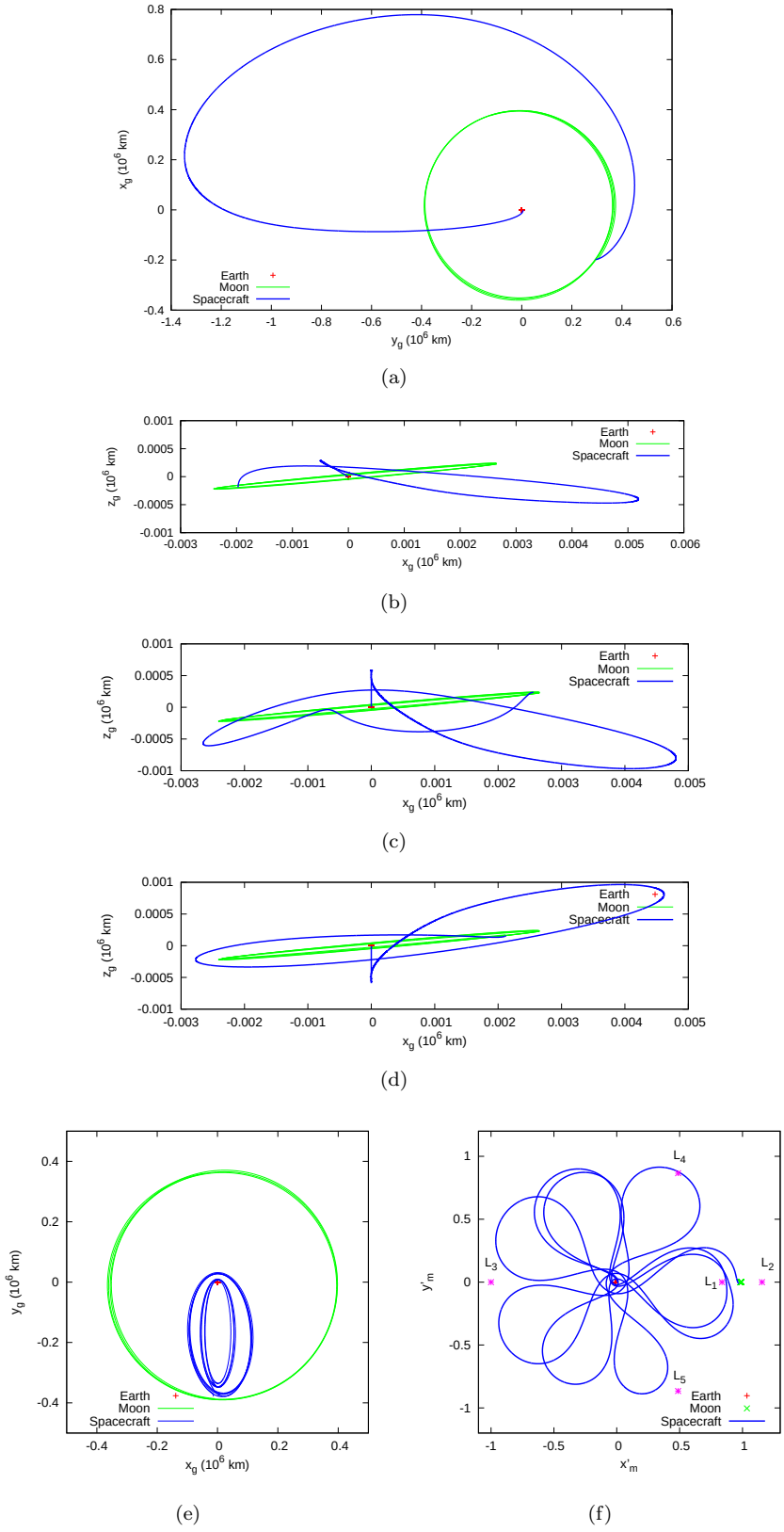

(a)

(b)

(c)

(d)

(e)

(f)

Fig. 8: (a): Typical outer transfer, $i = 0$, projection on the x-y plane; (b): x-z plane projection of another outer transfer, $i = 30$; (c): outer transfer, $i = 90$, $\Omega = 0°$, x-z plane; (d): outer transfer, $i = 90$, $\Omega = 180°$, x-z plane; (e), (f): inner transfer in the inertial and fixed-Earth-Moon frames respectively, $i = 28.55$, both in their x-y planes.

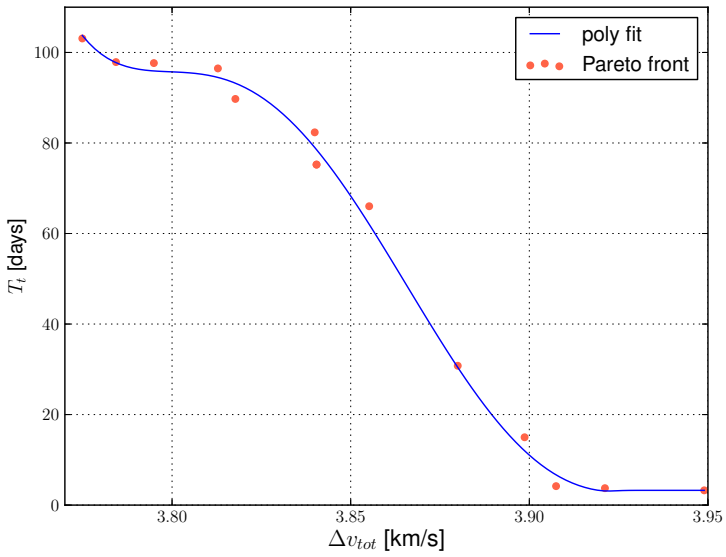

Fig. 9: The Pareto front in the Δv_{tot}-T_t plane and its 5^{th} order spline interpolation.

a large number of transfer orbits, like the one performed in this work, allows for the population of the objective space, where the objective functions are the Δv_{tot} and the transfer duration T_t. The Pareto set for this problem can be drawn with sufficient accuracy, as shown in Figure 9.

After the identification of the Pareto-optimal transfers, the next step in planning the mission is the investigation of the possible best choice of a single solution. This task is not easily automated because it depends, obviously, on the specific objectives and the restrictions of the mission. Examples of factors to consider would be i) the date of launch, ii) whether the mission is manned or unmanned, iii) the positions of Sun and Moon at the time of the first impulse, iv) the launch base, v) the launcher type and the method of propulsion, etc. All of these may be different for each mission project.

However, the choice of an optimal transfer can be simplified by means of multi-objective optimization techniques. In the next subsections this is done for the 2-objective problem of minimizing both the transfer duration and the total Δv, using part of the 7-dimensional search space formed by the initial spatial and velocity coordinates and the date of the first impulse.

5.2 Mapping of the Pareto Front Back to the Search Space

As a first step we analyse the location of the Pareto-optimal transfers in the space of the initial parameters.

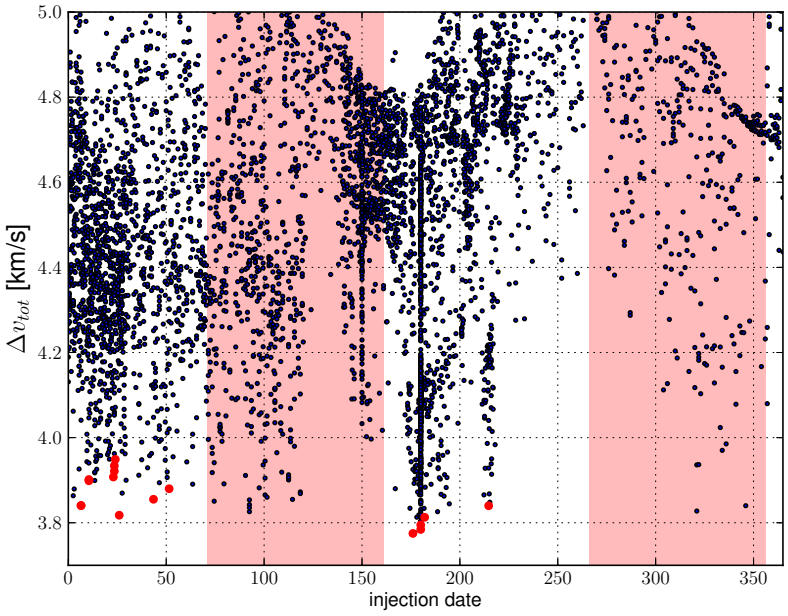

Fig. 10: Position of the points of the Pareto front (red dots) in the whole distribution by date of the orbits. The "unfavorable" quadrants (1^{st} and 3^{rd}) are shown on a darker background.

If the Pareto front is a continuous curve, it is expected that also its image in the search space is a continuous curve. Obviously, the more populated the Pareto front is, the more clearly the mapped set will be recognizable as a line. The front shown in Figure 9 is determined with 13 points only, and it is obtained from a partial exploration of the search space. In these conditions it is anyway possible to deduce valuable, although basic, information.

Figure 10 shows the position of the optimal points (in red) in the Δv_{tot}-"starting date" plane. The periods of time in which α is in its four quadrants is shown in white (2^{nd} and 4^{th}) and colored (1^{st} and 3^{rd}) background. All the optimal orbits fall inside the "favorable" (2^{nd} and 4^{th}) quadrants.

Figure 11 shows the same plot as Figure 3, that is, the relation between Δv_1 and Δv_2, but with the points corresponding to the Pareto front highlighted in red. As detailed in the previous sections, the Δv_1 is directly related to the apogee distance. In the plot, the points corresponding to the Pareto set are grouped into three distinct areas equivalent to the inner transfers ($\Delta v_1 < 3.1$ km s^{-1} i.e. apogees inside the orbit of the Moon), the Hohmann transfers ($\Delta v_1 = 3.1$ km s^{-1}, i.e. apogees equal to the Earth-Moon distance) and the outer transfers ($\Delta v_1 > 3.14$ km s^{-1}, apogees longer than 7×10^5 km).

The plot in Figure 12 is the distribution, again as a function of the Δv_1, of the distance between the spacecraft and the moon during the capture maneuver

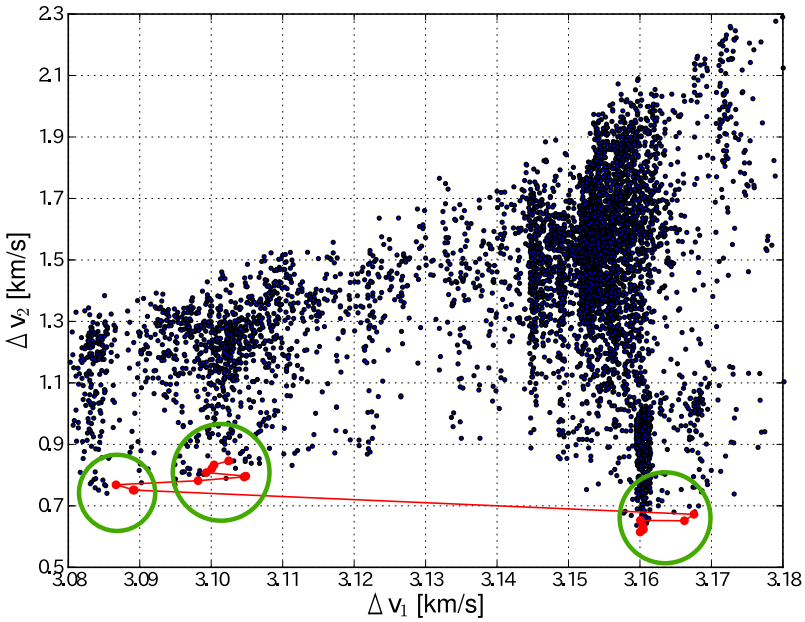

Fig. 11: The Pareto front (dots joined by the red line) in the Δv_1-Δv_2 plane. The line between the points shows the order in which they appear on the front (corresponding to increasing values of Δv_{tot}). The points occupy three distinct areas in the plane, highlighted by circles, corresponding to inner, Hohmann and outer transfers respectively from left to right.

Δv_2. The general distribution of orbits is random, as explained in the previous sections of this paper, and all the optimal transfers have capture distances close to 2000 km, which is the value that minimizes Δv for the final circularization [3]. This is not surprising, because that the final circularization maneuver contributes significantly to the total Δv.

5.3 Scaling Curve

As was pointed out earlier, there is no algorithm capable of giving a single optimal solution for all mission types, and the final decision rests with the humans performing the optimization. Nevertheless, there are several techniques that aid the decision-maker in his choice. One of these is the "weighting method", in which a weight is given to each objective based on its perceived importance. A function expressing the distance between the optimal points and a previously selected "ideal" or "utopia" point is minimized. Here we use the simple euclidean distance, or $L_{(2)}$ norm, between a generic point $(x_1(p), x_2(p))$ and the utopia point (x_1^*, x_2^*). The

[3] In fact the final orbit around the Moon has a radius of 2000 km.

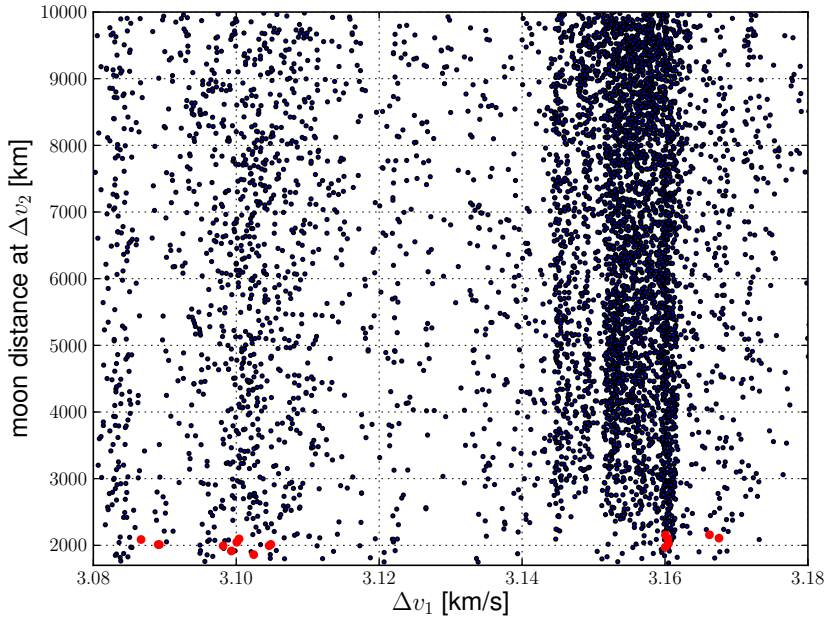

Fig. 12: The Pareto front (red points) in the distribution of distances from the Moon at injection, in relation to Δv_1.

$L_{(2)}$ norm is defined as:

$$d_{12} = \left[\left(x_1(p) - x_1^* \right)^2 + \left(x_2(p) - x_2^* \right)^2 \right]^{\frac{1}{2}} \tag{4}$$

The utopia point adopted here is the origin, ($\Delta v_{tot} = 0$, $T_t = 0$). Figure 13 shows how different weighting choices deform the front and result in different optimal points being closest to the utopia point (in normalized units).

Clearly, the weighting method reduces the problem to a single-objective minimization process. However, it has the drawback of having to choose the weights before seeing the respective solution. In some cases a small change in the weights can result in large differences in the solution, and the decision-maker has a hard time finding a clear answer. This is partly solved by the "scaling method" developed by Kasprzak (2001). This method takes each point of the Pareto front and computes the weighting (or scaling) that would be necessary to make that solution the closest one to the utopia point.

The general procedure used in the scaling method is as follows:

- fit the Pareto optimal set with a high-order polynomial or a spline curve;
- for each point in the curve, find the local slope m;
- compute the rescaling necessary to make the slope normal to the distance vector that must be minimized; the relation is $k = -m^{-1}$.

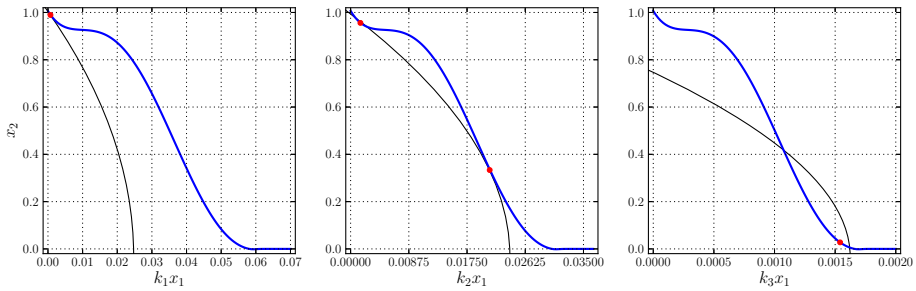

Fig. 13: Examples of three different weights for the objective functions and the consequent different optimal solutions. The axes are normalized for easier handling. Here the x_1-axis is deformed for easier viewing, so that the front appears to have the same shape, while the circumferences of constant distances (in black) appear to be ellipses with different eccentricities.

The result is a curve relating one of the objective functions to the scaling that leads to optimality. For example, by looking at Figure 13, we see that the curve would have (in the normalized units) a value of $k_1 = 0.07$ for the red point shown in the first graph, $k_2 = 0.036$ for the two points in the second graph and $k_3 = 0.002$ for the point in the third graph. The full curve, expressed in the original, physical units, is shown in Figure 14.

The scaling curve obtained in this way facilitates the decision-maker's job, because he now has information covering the whole spectrum of solutions, including the sensitivity to a change of weighting. The fact that in some cases more than one Pareto point corresponds to the same k scaling means that there are multiple solutions with the same distance to the utopia point and thus identically optimal, like for k_2 in Figure 13. However, the concave part of the front is never optimal in the weighting method. Its points never minimize the distance to the utopia point. This can be seen in the middle plot in Figure 13, where the whole arc between the two red dots is clearly unreachable by the circumference. All points of this kind are shown as a dashed curve in Figure 14 and should be excluded from the optimization procedure.

Practical application. The scaling k in Figure 14 can be interpreted physically as the number of days of transfer that have, for the specific purposes of the mission at hand, the same impact as a Δv_{tot} of 1 km/s.

For example, on a manned mission, 1 day of flight might be as expensive, in terms of security and costs, as 1 km/s of the total Δv. Using Figure 14, we look for the point in the curve that has $k = 1$ days/(km s^{-1}). Since we have the whole scaling curve, our choice of k need not be only one, but can be a range of values. In this case we see that the best solution would be for $\Delta v_{tot} > 3.91$ km/s. From this, using the Pareto front, we find that the best transfer orbits are the traditional Hohmann transfers.

On the other hand, transfer duration may have a much lower cost for an unmanned mission with science purposes, with a desired scaling $k \simeq 25$ days/(km s^{-1}).

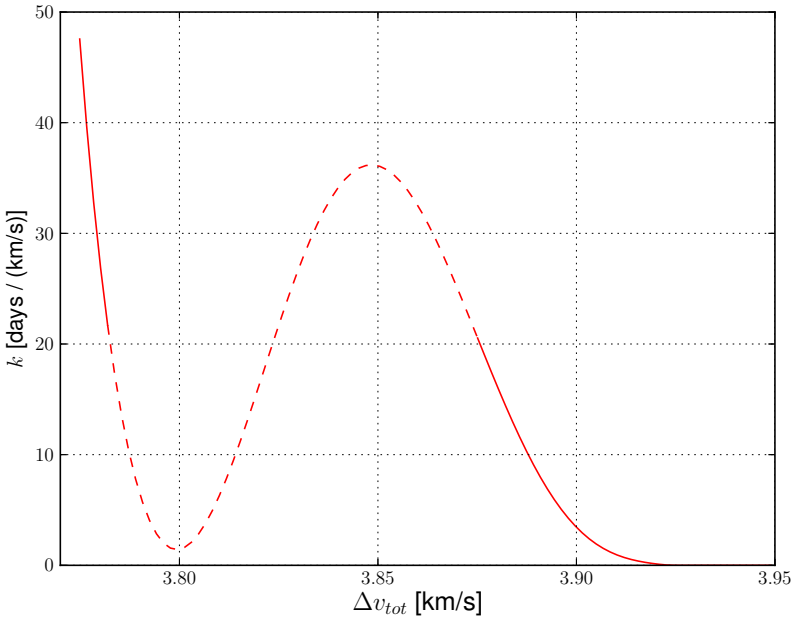

Fig. 14: The scaling curve resulting from the Pareto front in Figure 9 and a utopia point at the origin. The dashed part denotes non-optimal solutions.

In this case the optimal choice would be a low-energy orbit with $\Delta v_{tot} \simeq 3.78$ km/s and (from the Pareto front) $T_t \simeq 95$ days.

After locating an optimal transfer (or several candidates) on the front, mapping back to the search space gives its initial parameters like launch date, inclination and Δv_1.

6 Conclusions

In this paper we study the existence and characteristics of low- and high energy transfer orbits from the Earth to the Moon in the combined field of Earth, Moon and Sun. A wide-ranging and numerically precise study of these orbits contributes to a better understanding of the orbital dynamics. Among these transfers, low-energy orbits give clear advantages in terms of mission costs. A result of this work is that it is easy to obtain successful low-energy orbits just by properly setting orbital initial conditions, without resorting to mid-course maneuvers as, for instance, was the case for the Hiten spacecraft (Belbruno and Miller, 1990).

On the other side, this work has not the scope of a deep understanding of the underlying dynamical characteristics of these orbits, which is better studied by semi-analytical or geometrical approaches, like for instance the elegant techniques involving invariant manifolds (Koon et al, 2000; Gomez et al, 2002; Koon et al,

2008). In particular, it was shown how it is possible using invariant manifold techniques to construct low energy transfer paths to the Moon (Koon et al, 2001).

The existence of such orbits relies strongly on the help of the Sun, and the statistics show that a specific range of positions is required for the Sun for the practical realization of low-energy orbits, confirming previous results (Circi and Teofilatto, 2001). Another relevant result of this paper is the information about the range of apogee distances which most likely produce two-impulse outer low-energy transfers, which is found to be 1.23×10^6 km $\leq r_a \leq 1.31 \times 10^6$ km. Moreover, the simulations show that the outer orbits are capable of reaching the Moon independently of the inclination of the initial parking orbits, unless they are retrograde.

As a relevant final point, we discussed the use of multi-objective optimization (MOO) methods for the choice of appropriate transfer orbits. The acquired data allow us to draw the shape of the Pareto frontier, which is the fundamental element of a complete MOO analysis. After determining the Pareto front (set of all the optimal points in the objective space) it is possible to map back those points onto the search space (that of initial conditions) to get the optimal orbit initial conditions (launch date, inclination and first velocity impulse Δv_1).

While, clearly, a general technique of resolution of the problem of finding a single optimal transfer orbit is not viable because of the variety of contrasting objectives, whose specific relevance is highly mission-dependent, we sketched that a suitable first approach is that of reducing the MOO to a two-objective problem. The two objectives are the total impulse Δv_{tot} and the transfer time duration T_t. Also in this simplified frame a high degree of indeterminacy remains due to that the scope of the mission suggest whether higher relevance is to be given to the amount of injected impulse or to the transfer time.

The final tool used in the selection of a single optimal transfer is the scaling curve. The scaling curve shows the best choice given any T_t–Δv_{tot} preference factor k, which is mission dependent. We explore two different hypothetical cases of manned and unmanned missions. We find, choosing a $k = 1$ day/(km s^{-1}) for the sake of a manned mission, that optimal orbits are those with $\Delta v >$ 3.91 km s^{-1} which coincide with usual Hohmann orbits, while the request of $k \sim 25$ days/(km s^{-1}), quite reasonable for unmanned missions, leads to a low energy orbit as optimal, with $\Delta v \simeq 3.78$ km/s and $T_t \simeq 95$ days.

Acknowledgements We thank prof. Teofilatto (Sapienza, University of Roma, Italy) for useful discussions during the preparation of this paper.

References

Belbruno E (1987) Lunar capture orbits, a method of constructing earth moon trajectories and the lunar gas mission. In: 19th AIAA/DGLR/JSASS International Electric Propulsion Conference, Colorado Springs, Colorado, AIAA-87-1054

Belbruno E (2004) Capture Dynamics and Chaotic Motions in Celestial Mechanics. Princeton University Press

Belbruno E (2008) Resonance transitions associated to weak capture in the restricted three-body problem. Advances in Space Research 42(8):1330–1351

Belbruno E, Marsden BG (1997) Resonance Hopping in Comets. The Astronomical Journal 113:1433

Belbruno E, Miller J (1990) A ballistic lunar capture trajectory for japanese spacecraft hiten. Internal document JPL IOM 312/90.4- 1731, Jet Propulsion Lab., Pasadena, CA

Belbruno EA, Miller JK (1993) Sun-perturbed earth-to-moon transfers with ballistic capture. Journal of Guidance Control and Dynamics 16(4):770–775

Bello Mora M, Graziani F, Teofilatto P, Circi C, Porfilio M, Hechler M (2000) A systematic analysis on weak stability boundary transfers to the moon. In: Proceedings of 51st Inter. Astronautical Congress, Rio de Janeiro, Brazil

Capuzzo-Dolcetta R, Mastrobuono-Battisti A, Maschietti D (2010) Nbsymple, a double parallel, symplectic n-body code running on graphic processing units. New Astronomy 16(4):284–295

Cartwright JHE, Piro O (1992) The Dynamics of Runge-Kutta Methods

Circi C, Teofilatto P (2001) On the dynamics of weak stability boundary lunar transfers. Cel Mec Dyn Astr 79:41–72

Conley CC (1968) Low energy transit orbits in the restricted three-body problem. SIAM J Appl Math 16(4):732–746

Gomez G, Koon W, Lo M, Marsden J, Masdemont J, Ross S (2002) Invariant manifolds, the spatial three-body problem and petit grand tour of jovian moons. In: Scientific W (ed) Libration Point Orbits and Applications

Han SC, Mazarico E, Rowlands D, Lemoine F, Goossens S (2011) New analysis of lunar prospector radio tracking data brings the nearside gravity field of the moon with an unprecedented resolution. Icarus 215(2):455 – 459, DOI 10.1016/j.icarus.2011.07.020

Kasprzak EM (2001) Pareto analysis in multiobjective optimization using the colinearity theorem and scaling method. Structural and Multidisciplinary Optimization 22(3):208–218

Kawaguchi J, Yamakawa H, Uesugi T, Matsuo H (1995) On making use of lunar and solar gravity assists in lunar-a, planet-b missions. Acta Astronautica 35(9-11):633 – 642

Kinoshita H, Yoshida H, Nakai H (1991) Celes. Mech. and Dynam. Astr. 50, 59

Koon W, Lo M, Marsden J, Ross S (2000) Heteroclinic connections between periodic orbits and resonance transitions in celestial mechanics. Chaos 10:427469

Koon W, Lo M, Marsden J, Ross S (2001) Low energy transfer to the moon. Celestial Mechanics and Dynamical Astronomy 81:63–73

Koon W, Lo M, Marsden J, Ross S (2008) Dynamical Systems, the Three-Body Problem and Space Mission Design. Marsden Books

MacKay RS (1992) Some aspects of the dynamics and numerics of Hamiltonian systems. In: Broomhead DS, Iserles A (eds) The Dynamics of Numerics and the Numerics of Dynamics, Clarendon Press, Oxford, no. 34 in The Institute of Mathematics and Its Applications Conference Series, pp 137–193

Menyuk C (1984) Some properties of the discrete Hamiltonian method. Physica D: Nonlinear Phenomena 11(1-2):109–129

Miettinen K (2001) Some methods for nonlinear multi-objective optimization. Lecture Notes in Computer Science 1993:1–20

Yoshida H (1990) Construction of higher order symplectic integrators. Phys Lett 150(5,6,7):262–268